Vol. 25, No. 2(2026) Alim26714

Ingeniería de alimentos

Revista Mexicana de Ingeniería Química

Model of the traditional *Totopo* baking process

Modelo del proceso tradicional de horneado de *totopos*

A.E. Sánchez-Chacón[1]*, V. Simón-Simon[1], J. F. Hernández Ramírez[2]

[1] *Instituto de Estudios de la Energía, Universidad del Istmo, Tehuantepec, Oax.*

[2] *Laboratorio de Ingeniería de Reactores Catalíticos (LIRC), Universidad Autónoma Metropolitana-Iztapalapa, Ciudad de México.*

Received: November 13, 2025; Accepted: April 1, 2026

Abstract

This study is based on a review of specialized food engineering literature to develop a model aimed at evaluating the influence of heat and mass transfer mechanisms in the traditional *totopo* baking process, with the purpose of identifying its distinctive characteristics. Experimental data obtained using infrared sensors were collected directly from monitoring the operation of traditional ovens. The model incorporates an evaporation kinetics term that couples the *totopo* differential mass and energy balances. This approach allows the experimental monitoring of the dough surface temperature to serve as an effective indicator to guide process modeling, while also enabling the independent treatment of mass transfer parameters for each phase. The model results show that radiation and contact heat transfer mechanisms together contribute approximately 75–80% of the total energy supplied to the *totopo*, while convection accounts for the remainder. The study also helps identify suitable instrumentation for use in an experimental traditional oven, allowing for a more accurate estimation of the contribution of these mechanisms. Regarding internal mass transport in the vapor phase, the model proposes an effective transport coefficient that combines the influence of temperature with a convective component associated with pressure gradients.

Keywords: baking model, corn *totopo*, heat transfer, mass transfer, comixcal.

Resumen

Este estudio se basa en la revisión de la literatura especializada en ingeniería de alimentos para desarrollar un modelo orientado a evaluar la influencia de los mecanismos de transferencia de calor y masa en el proceso de horneado de *totopos*, con fin de identificar sus características distintivas. Los datos experimentales se han obtenido mediante sensores infrarrojos en el monitoreo de la operación de hornos tradicionales. El modelo incorpora una cinética de evaporación que acopla los balances diferenciales de masa y energía en el totopo; este vínculo permite que el monitoreo experimental de la temperatura superficial de la muestra, sea un indicador eficaz para guiar la modelación del proceso, mientras posibilita, asimismo, el tratamiento independiente de los parámetros de transferencia de masa en cada fase. Los resultados del modelo muestran que la radiación y contacto térmico aportan conjuntamente del 75 a 80 % de la energía total transferida al *totopo*, mientras la convección contribuye con el resto. El estudio permite, asimismo, identificar la instrumentación a implementar en un horno tradicional experimental para una estimación más precisa de la contribución de estos mecanismos. En torno al transporte en fase vapor, se propone un coeficiente efectivo que combina la influencia de la temperatura con un componente convectivo asociado a los gradientes de presión.

Palabras clave: modelo de horneado, *totopo* de maíz, transferencia de calor, transferencia de masa, Comixcal.

*Corresponding author. E-mail: jonios4c@gmail.com ;

https://doi.org/10.24275/rmiq/Alim26714

ISSN:1665-2738, *issn-e*: 2395-8472

1 Introduction

The artisanal production of *totopos* in the Isthmus of Tehuantepec region, using dough prepared through the traditional nixtamalization process of Zapalote chico maize—a unique, locally adapted species developed over centuries—constitutes an essential activity within both the regional economy and cultural identity (López-Saynes, 2018). Conversely, on a global scale, the production of corn-based snack foods represents a multi-million-dollar and rapidly growing industry (Serna-Saldívar and Chuck-Hernández, 2019).

The development of Food Engineering is closely linked to advances in Process Engineering knowledge and methodologies (Welti-Chanes *et al*., 2005). One fundamental area in Process Engineering is Transport Phenomena and the modeling discipline derived from it. Chakraborty and Dash (2023) presented a comprehensive review on modeling approaches and transport mechanisms involved in the baking of food products. Several handbooks and specialized texts in Food Science and Engineering provide a general overview of drying and baking processes (Heldman *et al*., 2018; Varzakas and Tzia, 2014). Others focus on the conceptual framework of heat and mass transfer mechanisms (Dincer, 2010; Mittal, 2010). Additional works address the transport parameters associated with these processes (Saravacos and Maroulis, 2001; Krokida and Saravacos, 2013; Doulia *et al*., 2000; Rosentrater *et al*., 1999).

Drying and baking processes share some coupled heat-and-mass transfer mechanisms, differing mainly in the temperature ranges at which they are operated. In the discipline of food drying, boundary-layer theory has been widely used to characterize moisture transport (Erbay, Z., and Icier, F., 2010). Essentially, thin-layer theory is aimed at representing drying curves by monitoring the sample's total mass loss over time under constant airflow and temperature conditions. This experimental data is subsequently utilized to fit the parameters of semi-empirical equations or models—frequently derived from Fick's Second Law of Diffusion—to describe moisture transport within the liquid phase.

Current research reflects a significant trend toward the precision monitoring and mathematical modeling of drying kinetics in food matrices. For instance, Gutiérrez-Martínez *et al*. (2024) demonstrated the efficacy of coupling digital and thermal imaging to monitor real-time surface temperature and shrinkage in potato slices, using Fick's second law and Fourier's approach to characterize thermal kinetics. Similarly, Loan *et al*. (2025) employed semi-empirical models, such as the Page equation, to determine moisture diffusivity and activation energy during the dehydration of germinated rice, even incorporating artificial neural networks to enhance predictive accuracy.

While these studies provide a robust framework for convective drying—where air flow is the primary vehicle for heat transfer—they are fundamentally anchored in thin-layer theory, which often assumes uniform processing environments. However, traditional artisanal processes, such as the baking of totopos in clay ovens, diverge significantly from these controlled convective scenarios. In such cases, the interaction between the food and the heating source is dominated by radiation and contact mechanisms rather than convection alone. Consequently, there is a critical need for coupled mass and energy balance models that can account for these complex heat transfer contributions while maintaining the independent treatment of mass transfer parameters for each phase.

Regarding modeling studies on the baking of tortilla chips, Kayacier and Singh (2004) analyzed the prediction of liquid-phase moisture content using an approach derived from Fick's second law. Experimental data on mass loss during baking were used to estimate a constant effective diffusivity value for each baking temperature, with reported values ranging from 6.25×10^{-10} m^2/s (450 K) to 1.097×10^{-9} m^2/s (600 K). An Arrhenius-type dependence of the effective diffusivity on temperature was proposed, with the activation energy and reference diffusivity obtained through regression of experimental data.

Xu and Kerr (2012) modeled the moisture loss of tortilla chips in a vacuum dryer. Their semi-empirical model described liquid-phase moisture transport according to Fick's second law with a constant effective diffusivity coefficient representing the combined effects of multiple mass transfer mechanisms, including surface diffusion, capillary diffusion through narrow tubular structures, Knudsen diffusion, and gas-phase transport driven by pressure or concentration gradients. Reported effective diffusivity coefficients were on the order of 10^{-9} m^2/s at temperatures between 80 and 100 °C. Based on these data, Arrhenius-type parameters (Peters *et al*., 2002) were evaluated for the temperature dependence of the coefficient.

Iribe-Salazar *et al*. (2018) modeled mass transfer during the baking of corn tortillas. Pre-cooked tortillas were baked in a commercial electric oven at 180 °C for 600–650 s. Comparison between the model predictions and experimental data of the moisture evolution curves over time showed better agreement when the effective diffusivity coefficient was estimated through successive pointwise approximations. The instantaneous values ranged from 10^{-10} m^2/s at the beginning to 1.4×10^{-9} m^2/s at 650 s, outlining a smooth curve.

Feyissa *et al*. (2011) published a study that introduced the phase change from liquid to vapor within the sample domain through a heterogeneous first-order Arrhenius-type reaction. The model, developed for the baking of pancakes, included a differential energy balance and mass balances for both liquid- and vapor-phase moisture. Constant effective diffusion coefficients were assumed, with values of 10^{-9} m^2/s for the liquid phase and 8×10^{-7} m^2/s for the vapor phase (Thorvaldsson & Janestad, 1999).

In a broader context, several studies can be cited. Cevoli *et al*. (2020) focused on estimating the liquid-phase effective diffusivity during cake baking, incorporating the use of numerical solution software and correlations for estimating convective mass and heat transfer coefficients. Likewise, Ousegui *et al*. (2010) investigated bread and baguette baking using a porous-medium transport approach that included evaporation within the sample domain. This study emphasized the importance of capillary diffusion for the liquid phase and described vapor-phase transport as driven by total pressure and concentration gradients.

Regarding external heat transfer, Demirkol *et al*. (2006) presented a model and experimental setup to evaluate convective heat transfer coefficients during cookie baking. Their approach was based on the experimental estimation of heat flux using a thin-layer sensor and on the dough's mass loss. Reported surface convective coefficients ranged from 30 $W/m^2{\cdot}K$ under natural convection at a baking temperature of 190 °C to 42 $W/m^2{\cdot}K$ under forced convection at 210 °C.

Similarly, Carson *et al*. (2006) proposed several approaches for experimentally determining the convective heat transfer coefficient under different flow and equipment conditions. The study established a range of values between 15 and 40 $W/m^2{\cdot}K$, attributing a partial contribution to radiation. Furthermore, the experimental data provided by the authors allowed the estimation of mass transfer coefficients as functions of vapor pressures at the interface and partial pressure in air. A typical reported value was 2.4×10^{-6} $mol/m^2{\cdot}s{\cdot}Pa$, or equivalently 5.9×10^{-3} m/s when expressed in terms of concentration differences.

The works cited in this background review constitute a selection of those that have guided the modeling strategies and parameter assessments employed in this study.

2 Description and basic characterization of the traditional *totopo* oven

In the work of López Saynes *et al*. (2018), a general description of the traditional oven, or Comixcal, is provided. It consists of a ceramic pot placed within a receptacle built with brick and clay walls (Figure 1). The space between the pot and its container is filled with sand and gravel, which serve as insulation. The pot typically has a spheroidal shape. In a representative oven, such as those observed in the field tests, the polar and equatorial axes measure approximately 60 cm. Since the construction is entirely artisanal, the pots tend to be slightly flattened at the poles.

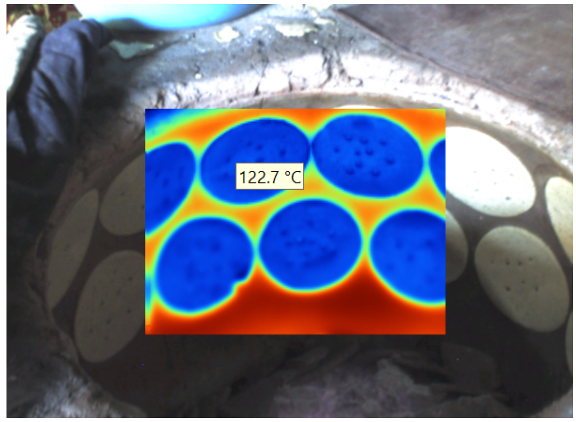

Figure 1. Traditional *totopo* oven: thermal camera image showing the infrared view in the inset.

In this study, the experimental information was gathered through direct observation and monitoring of traditional oven operation. The equipment used included a Fluke Ti40 IR Fusion Technology thermal camera, a Fluke 64 infrared sensor (to extend the measurement range to ember temperatures), and a digital sensor with a type-K thermocouple to estimate the temperature of the gaseous atmosphere inside the oven. A brief characterization of the operation of the traditional *totopo* oven is presented below.

Firewood is placed inside the oven at its flat lower base, which has a diameter of approximately 40 cm, and is ignited for the preparation of nixtamal. Once this stage is completed, the glowing embers are used for the baking of *totopos* over several hours, typically 6 to 8 h. At the beginning of the operating period, the embers are partially covered with fragments of ceramic, which are gradually removed from the central area as the hours pass. Oxygen supply and the release of air and combustion gases occur through an opening of approximately 45 cm in diameter at the top of the oven. A metal sheet is used to cover this opening; however, it does not seal tightly and allows gas flow by natural convection. The cover is removed intermittently to introduce or remove the *totopos*.

During the baking process, the molded dough, with a diameter of 14 cm and a weight between 40 and 42 g, is manually adhered to the inner surface of the oven, where it receives heat by contact. The opposite surface is exposed to radiation from the embers (located at the bottom of the oven, with surface temperatures ranging from 500 to 600 °C, and partially covered by ceramic fragments at 250–300 °C) and to convection from the gaseous phase composed of air and combustion gases. The gas-phase temperature varies from an average of approximately 190 °C, increasing near the ember zone and decreasing toward the upper opening. The dough gradually increases in temperature and loses moisture until it is fully released at the end of the baking period, when the exposed surface reaches approximately 220 °C.

In the field sessions recorded for this study, each batch of *totopos* consisted of 25 units distributed on two levels: the lower level, closer to the embers, and the upper level (Figure 1). The baking period observed in these sessions ranged from 16 to 17 minutes for the oven lower and upper levels, respectively, with resting intervals of at least 5 to 10 minutes between successive batches to allow recovery of the oven surface temperature. The internal surface temperatures measured immediately before loading a new batch varied from approximately 230 °C near the ember zone to 200 °C in the upper area. Upon contact with the moist dough, the surface temperature dropped abruptly and evolved throughout the baking period, reaching values of about 150–160 °C at the time of removal.

Concluded the sections on background and oven characterization, the next part of this study focuses on the description and formulation of the proposed physical and mathematical model for the traditional *totopo* baking process.

3 Equations of the model

The formulation of the model was developed considering a two-dimensional conception. Figure 2 shows the axi-symmetric geometry of the *totopo* in the r–z coordinates, along with the transport mechanisms involved in the process. The dough disc has a diameter of 14 cm and a mass ranging from 40 to 42 g. Assuming a corn masa density of 1150 kg/m^3, the mean thickness of the disk, L_c, is approximately 2.3 mm.

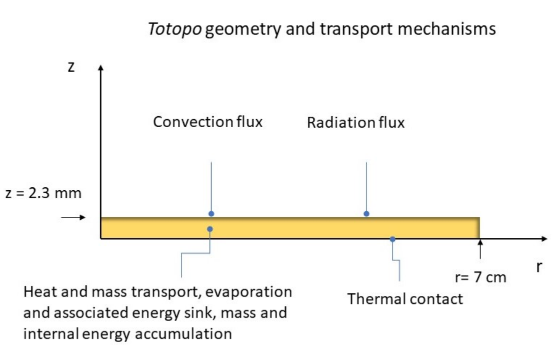

Figure 2. *Totopo* geometry and transport mechanisms.

The thermal energy balance for the *totopo* considers the accumulation of internal energy, the heat flux by conduction $\vec{q}$, and a heat sink Q resulting from the liquid–vapor phase change within the sample. Effective thermal conductivity (k) and specific heat capacity (c_p) are expressed as functions of the local moisture (Krokida and Saravacos, 2013; Rosentrater *et al*., 1999), evaluated at a process mean temperature:

$$\rho c_p \frac{\partial T}{\partial t} + \nabla \cdot \mathbf{q} = Q, \tag{1}$$

$$\mathbf{q} = -k\nabla T \tag{2}$$

The initial condition corresponds to the uniform temperature of the dough at the moment it is placed into the oven, throughout the domain:

$$\text{at } t = 0, \quad T = T_0 = 25°C \tag{3}$$

Boundary conditions assume axial symmetry with no heat flux at $r = 0$. Convective and radiative fluxes are imposed on the surfaces exposed to hot gases and embers. The convective heat transfer coefficient (h) ranges between 15 and 30 W/m^2·K, Carson *et al.* (2006), while the radiative heat flux (*fluxr*) reaching the *totopo* is estimated in magnitude order of 2000 W/m^2, based on the geometry of the system and measured temperatures of the embers and ceramics (Cengel and Ghajar, 2015; Urban *et al*., 2019). The thermal contact between the *totopo* surface and the oven wall at $z = 0$ is modeled using a thermal resistance concept represented by a convective coefficient. h_T:

$$\text{at } r = 0, \quad k\frac{\partial T}{\partial r} = 0, \tag{4}$$

$$\text{at } z = L_c, \quad k\frac{\partial T}{\partial z} = h(T_a - T) + fluxr, \tag{5}$$

$$\text{at } r = R, \quad k\frac{\partial T}{\partial r} = h(T_a - T) + fluxr, \tag{6}$$

$$\text{at } z = 0, \quad -k\frac{\partial T}{\partial z} = h_T\,(T_{sh} - T). \tag{7}$$

The inner wall temperature of the oven T_{sh} (t) was modeled using a time-dependent temperature following partial experimental data. The coefficient h_T is adjusted to account for the sudden increase in the surface temperature of the *totopo* upon contact with the oven wall, followed, later, by the partial loss of direct contact between the dough disc and the oven surface. Here, $t_p$denotes the baking time, while h_{To} and n are fitting parameters:

$$h_T = h_{To}\left(1 - \left(\frac{t}{t_p}\right)^n\right) \tag{8}$$

The mass balance accounts for accumulation, evaporation rate (R_{evap}), and the mass fluxes associated with liquid and vapor phases. The local concentrations of liquid and vapor moisture are denoted as c and c_v , respectively:

$$\frac{\partial c}{\partial t} = \nabla \cdot \left(D_{efL} \nabla c\right) - R_{evap} \tag{9}$$

$$\frac{\partial c_v}{\partial t} = \nabla \cdot \left(D_{efv} \nabla c_v\right) + R_{evap} \tag{10}$$

In the liquid phase, the initial condition corresponds to a uniform moisture concentration c_0. Boundary conditions for moisture assume axial symmetry with no mass flux at $r = 0$:

$$\text{at } t = 0, \quad c = c_0 \tag{11}$$

$$\text{at } r = 0, \quad \frac{\partial c}{\partial r} = 0 \tag{12}$$

Liquid-phase moisture flux at the totopo surfaces is not considered. The kinetic formulation of liquid–vapor phase change, R_{evap}, allows an adequate coupling between internal and external moisture transport, naturally occurring in the vapor phase.

The transport of liquid-phase moisture is represented in terms of an effective diffusivity coefficient D_{efL} associated with capillary diffusion in the porous structure (Ousegui *et al*., 2010). This is expressed using a reference diffusivity D_{ref}, a fitting parameter, and the local moisture loss fraction, where ρ represents the local density of the *totopo*:

$$D_{efL} = D_{ref} \left[\frac{(\rho_0 - \rho)}{(0.6\,\rho_0)}\right] \tag{13}$$

In the vapor-phase, the initial is established by a uniform moisture concentration c_{v0}. Boundary conditions for moisture assume axial symmetry with no mass flux at $r = 0$:

$$\text{at } t = 0, \quad c_v = c_{v0} \tag{14}$$

$$\text{at } r = 0, \quad \frac{\partial c_v}{\partial r} = 0 \tag{15}$$

At the surfaces, internal fluxes are coupled with convective fluxes for the vapor phase. Here, k_m is the up-surface mass transfer coefficient: magnitude order between 10^{-2} and 10^{-3} m/s, based on mass transfer correlations and Chilton Colburn analogy (Cengel and Ghajar, 2015); and experimental data presented by Carson *et al*. (2006). Mass transfer in down-surface is modeled considering the experimental observations showing evaporation in thus surface caused by the irregular inner over surface. The model coefficient k_{mc} includes the influence of the flux originated by pressure gradients between the contact area and oven inner atmosphere. c_{bulk} is the atmosphere vapor concentration.

$$\text{at } z = L_c, \quad -D_{efv} \frac{\partial c_v}{\partial z} = k_m (c_v - c_{bulk}) \tag{16}$$

$$\text{at } r = R, \quad -D_{efv} \frac{\partial c_v}{\partial r} = k_m (c_v - c_{bulk}) \tag{17}$$

$$\text{at } z = 0, \quad D_{efv} \frac{\partial c_v}{\partial z} = k_{mc} (c_v - c_{bulk}) \tag{18}$$

For vapor-phase transport, an effective transport coefficient is proposed:

$$D_{efv} = D_{efT} + D_{efp} \tag{19}$$

D_{efT} coefficient accounts for the temperature effect, following an Arrhenius-type dependence with activation energy E_{ad} (Kayacier *et al*., 2004). The influence of local pressure gradients in moisture vapor phase is considered introducing the coefficient D_{efp}:

$$D_{efT} = D_0 \exp\left(\frac{E_{ad}}{R\,T}\right) \tag{20}$$

$$D_{efp} = D_{op}\left(\frac{abs(gradPz)}{gradPo}\right) \tag{21}$$

In these expressions, R is the universal gas constant and D_0 is the reference diffusion coefficient in the Arrhenius expression. In turn, D_{op} represents the reference coefficient associated with the pressure gradient, and $gradPo$ is a reference constant parameter.

The phase-change kinetics (liquid–vapor) follows a heterogeneous first-order Arrhenius-type reaction (Thorvaldsson & Janestad, 1999; Feyissa *et al*., 2011; Peters *et al*., 2002), with activation energy E_a. Essentially, Equation (4) defines the local evaporation rate R_{evap} as a function of liquid moisture concentration (c), temperature (T), and evaporation temperature (T_{evap}). The parameter K_{evap} can be used as a fitting parameter, and the factor f_T modulates the kinetics to attenuate evaporation below T_{evap}. The local rate of evaporation

$$R_{evap} = K_{evap}\, c\, f_z\, f(T, T_{evap}) \tag{22}$$

$$f\left(T,\, T_{evap}\right) = \exp\left[\frac{E_a}{R\,T}\left(\frac{1}{(f_T\,T)} - \frac{1}{T_{evap}}\right)\right] \tag{23}$$

The effect of void fraction in the evaporation rate is introduced by the f_z *(z)* function that improves evaporation rates away from the central region. z_c is the half *totopos* thickness. Constants a and b are fitting parameters.

$$f_z = \left(abs\left(\frac{(z - z_c)}{z_c}\right)\right)^a + b \tag{24}$$

The evaporation kinetics provide the coupling between mass and energy balances. The heat sink Q resulting from phase change is simply the product of the evaporation rate and the latent heat of vaporization λ:

$$Q = \lambda\, R_{evap} \tag{25}$$

The model implementation and numerical solution were performed using COMSOL Multiphysics. The *totopos* prepared in the ovens studied have a diameter of 14 cm and an average thickness of 2.3 mm.

Table 1.- Model base case parameters

Initial density ρ_0 = 1150 [Kg/ m^3] Initial temperature To = 298.15 [K] Liquid water initial concentration: $\mathbf{c_0}$ = 38 330 [mol/m^3] Vapor initial concentration: $\mathbf{c_{v0}}$ = 40.9 [mol/m^3] (1 atm 25°C)	Radiation flux *fluxr*= 1900 [W/m^2] Heat transfer coefficient h =*25 [W/(m^2·K)]* Thermal resistance parameter: h_{To}= 200 [W/(m^2·K)] Thermal resistance parameter n = 0.75 Gases bulk temperature Ta =453.15 [K]
Density $\rho = 0.4\,\rho_0 + PM\,(c + c_v)$ [Kg/ m^3] Thermal conductivity and Heat capacity: $\mathbf{k}$ = 0.27 + 0.38 m [W / (m K)] (*) $\mathbf{c_p}$ = 1520 + 2720 m [J / (kg K)] (*) Liquid mass fraction: $m = (PM\,c) / (PM\,c + 0.4\,\rho_0)$ (*) (Krokida & Saravacos, 2013)	Liquid reference diffusivity D_{ref} = 8e-7 [m^2/s] Vapor reference coefficient D_o= 5e-5 [m^2/s] Vapor reference coefficient D_{oP} = 2.4e-6 [m^2/s] Activation energy E_{ad} in D_{efT} = 13400 [J/mol] (Kayacier *et al*., 2004) Reference pressure gradient: *gradPo* = 8.81e7 [N/m^3]
Kinetics parameter $\mathbf{K_{evap}}$ =8.1e-3 [s^{-1}] Activation energy: $\mathbf{E_a}$ = 41400 [J/mol] (Feyissa *et al*., 2011) Kinetics inhibition parameter $\mathbf{f_T}$ = 0.92 Function $\mathbf{f_z}$ parameters a= 3 b=0.5 Evaporation heat λ = 2.3e6 [J/kg]	Vapor mass transfer coefficient surface up k_m = 0.004 [m/s] Vapor mass transfer coefficient surface down: k_{mc}= 0.016 [m/s] Vapor concentration c_{bulk} = 25.75 [mol/m^3] (1atm 200 °C)

To mitigate the geometric disproportion in the numerical meshing, a diameter of 8 cm was used in the simulation.

Experimental data and observations, collected during monitoring of a traditional totopo oven, provided essential feedback that guided model development and parameter estimation. Having established the model formulation, selected illustrative results are presented.

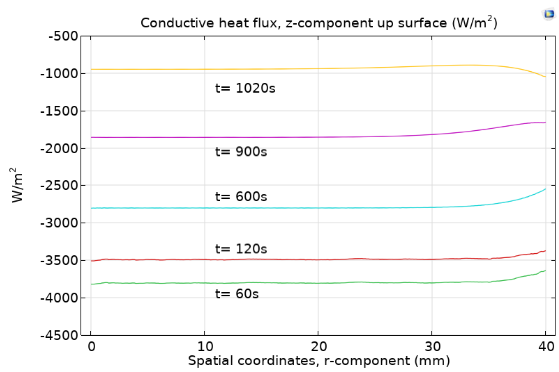

Figure 3. z-component of the diffusive heat flux on the *totopo* surface exposed to air and combustion gases in the oven.

4 Results and discussion

The results associated with a base case illustrating the significant variables and parameters of the model are presented first. Table 1 shows the values of the parameters that define this case. Some variants are discussed afterward.

During the baking process, the *totopo* is subjected to various heat transfer mechanisms. Figure 3 shows the diffusive heat flux on the surface in contact with air and combustion gases. This flux represents, at the boundary of the sample domain, the energy received through convection and radiation mechanisms acting on that surface. This plot allows us to evaluate the relative contribution of these mechanisms as a function of time during the baking period, considering that the radiative flux remains constant throughout this interval.

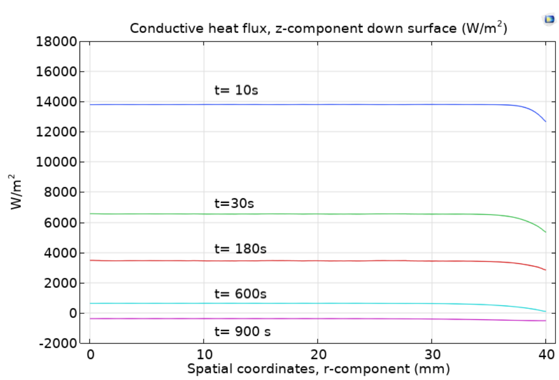

Figure 4. z-component of the diffusive heat flux on the *totopo* surface in contact with the oven's inner wall.

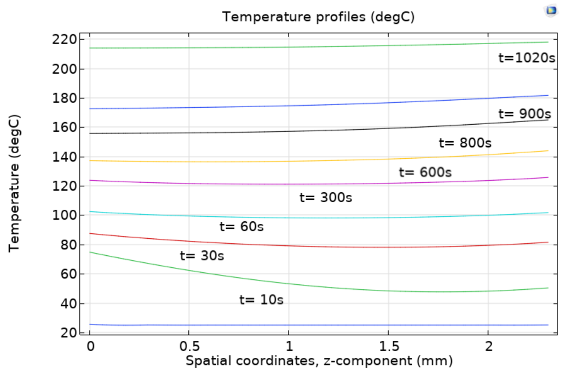

Figure 5. Evolution of temperature profiles along z during the 17-minute baking period.

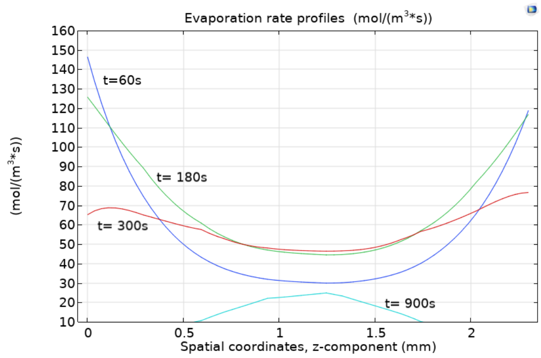

Figure 6. Evolution of evaporation-rate profiles along z in the *totopo*.

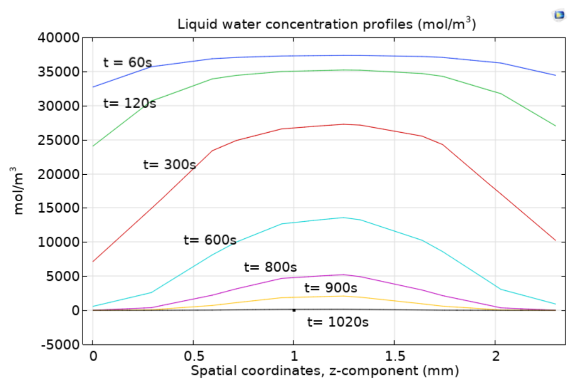

Figure 7. Evolution of liquid-phase moisture profiles in the *totopo*.

Another significant energy input arises from direct contact with the inner surface of the oven (Figure 4). A substantial energy input is observed during the initial period, which decreases as the *totopo* surface temperature increases. Overall, in the energy balance, the contribution of each heat transfer mechanism is as follows: radiation, 9741 J (46%); contact, 7282 J (34%); and convection, 4345 J (20%). These values correspond to a *totopo* of 8 cm in diameter as defined in the model. The contribution from the peripheral surface, on the order of 1% for an original dough disk, is not included.

The evolution of temperature profiles in the totopo (Figure 5), reflects the interaction between external and internal energy-transfer mechanisms and the thermal effect associated with moisture phase change. At short times (< 60 s) the totopo temperature rises rapidly for two main reasons: (a) the large temperature difference between the oven walls or the hot gases and the totopo surfaces, and (b) the evaporation rate and its associated thermal effect remain low at these relatively low temperatures (< 100 °C). For times between 60 s and 600 s the temperature increase is slower and more gradual, because a substantial fraction of the supplied energy is consumed by the liquid-to-vapor phase change. Finally, for times > 600 s, as liquid-phase moisture decreases, the rate of temperature increase rises again, becoming more pronounced toward the end of the baking period when moisture concentration approaches zero. Moreover, except during the initial seconds—when the thermal effect of evaporation is negligible and the energy input via the three heat-transfer mechanisms is maximal—the temperature gradients across the totopo thickness are barely perceptible.

Figure 6 shows the evolution of evaporation-rate profiles along the z-coordinate (across the *totopo* thickness) during baking. The phase-change kinetics is activated by temperature and depends on the local liquid-phase moisture content and evaporation temperature. T_{evap}, this parameter is established by local pressure. The inclusion of an evaporation kinetics term within the sample domain is consistent with experimental observations showing that evaporation occurs beyond the *totopo* surfaces.

As evaporation (liquid-to-vapor phase change) reduces the liquid-phase moisture content, the observed concentration profiles (Figure 7) become controlled by the relatively slow internal mass transport (low effective diffusion coefficient), which limits the rate at which these gradients can be dissipated. The liquid water concentration curves tend toward zero by the end of the 17-minute baking period. Tests performed in a commercial oven on dough samples and freshly baked *totopos* confirmed total moisture loss.

The model introduces an effective vapor-phase transport coefficient that accounts for the effects of temperature and pressure gradients at the local level. Figure 8 shows the contribution of each mechanism as a function of time, represented by the average value within the *totopo* domain. During the initial minutes of the baking period, while the temperature is rising, pressure gradients have a more significant influence on vapor-phase moisture transport. Later, this situation reverses as pressure gradients weaken toward the end of the period.

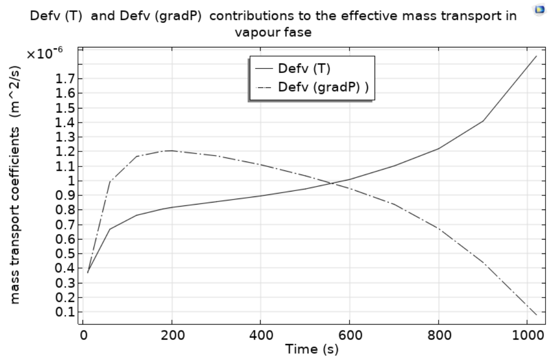

Figure 8. Contribution of temperature and pressure gradients to the effective vapor-phase transport coefficient.

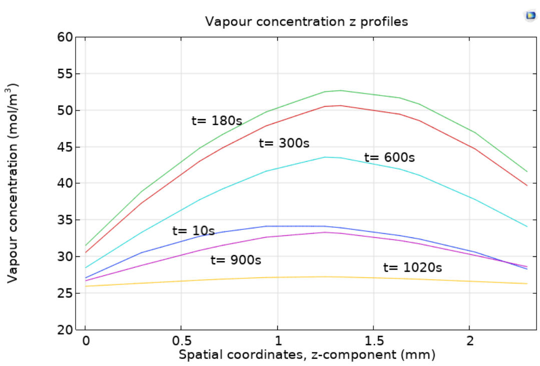

Figure 9. Evolution of vapor-phase moisture profiles concentration in the *totopo*.

The evolution of vapor-phase concentration profiles is shown in Figure 9. The vapor concentration rises to a peak visible in the profile at 180 s, where high temperatures coincide with elevated liquid-phase moisture concentrations. At later times, as the liquid-phase moisture is depleted, the vapor concentration decreases. The resulting concentration gradients follow the same behavior shown in Figure 7: they are governed by the interplay of evaporation and the relatively slow internal mass transport.

Figure 10 presents the model prediction for the surface temperature curve of *totopos* as a function of time during baking. Experimental data were included for two samples placed side by side on the upper level of the oven, captured through a sequence of thermal images. To acquire these images, the oven lid must be removed, which generates a transient convective airflow that produces a momentary cooling effect. This results in a slight temperature decrease that becomes cumulative when three or four measurements are taken during the baking period.

Toward the end of the baking process (around 900 s), as the liquid water fraction within the porous structure decreases, the *totopo* tends to crack and partially separate along its two faces. The experimental temperatures shown in Figure 10 represent the average of a range of surface

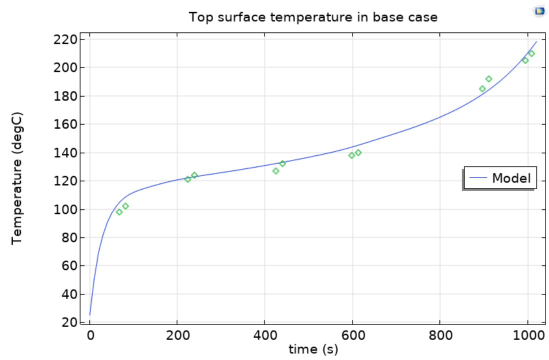

Figure 10. Surface temperature of a *totopo* on the upper oven level, base case.

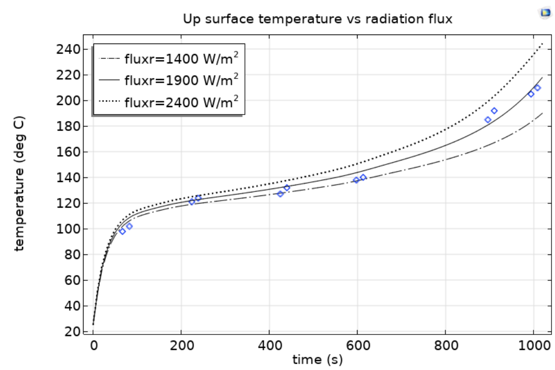

Figure 11. Effect of radiative flux on the surface temperature of the *totopo*, base case.

temperatures observed on the *totopo*; this range is typically between 4 and 8 °C but widens to 20 °C or more in the final baking phase (for times of about 800 s or longer) due to the spontaneous partial separation of the *totopo* from the oven's inner surface and the presence of zones with higher thermal resistance.

Figure 11 shows the effect of the radiative flux on the evolution of the surface temperature of the *totopo* exposed to the combustion gases. All other parameters defining the base case are kept constant. A more noticeable effect is observed toward the final phase of baking, where radiation becomes the dominant heat transfer mechanism to the *totopo*. In this stage, the reduction in the evaporation rate and the associated thermal effect also contributes.

The effect of the effective vapor-phase transport coefficient, D_{efv}, on the *totopo* surface temperature is shown in Figure 12. The reference is the base case value, illustrated in Figure 8. The additional curves show the effect of reducing this coefficient to one-half and one-quarter of its base value. It is observed that the influence of this transport parameter is less pronounced than that of the radiative flux. In contrast, its effect extends throughout the baking period: increasing this coefficient facilitates vapor transport toward the outer surface of the *totopo*, thereby reducing the vapor-phase moisture concentration and the associated evaporation temperature, and

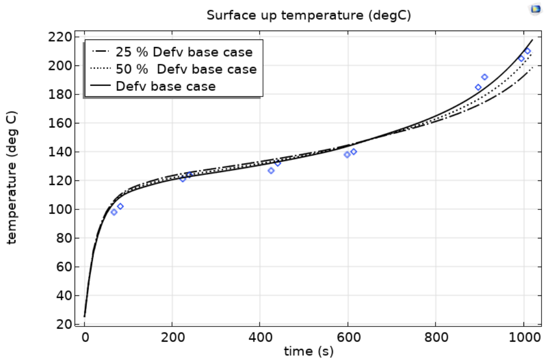

Figure 12. Effect of the effective internal mass transport coefficient D_{efv} on the *totopo* surface temperature.

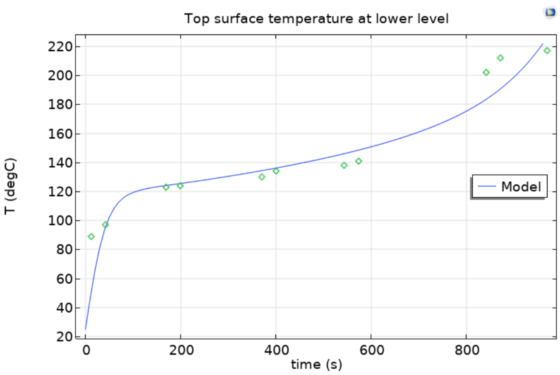

Figure 13. Surface temperature of a *totopo* on the lower oven level.

consequently promoting the liquid–vapor phase change.

Finally, Figure 13 presents a comparison between model predictions and experimental data for the surface temperature of a *totopo* located on the lower rack, near the base of the oven. In this region, the average gas temperature T_a increases to approximately 200 °C (compared to about 180 °C in the upper level). The temperature of the oven's inner surface, T_{sh}, also rises at the beginning of the baking period (around 220 °C), drops abruptly upon contact with the moist dough as evaporation begins, and later increases again to about 160 °C when the *totopo* is removed.

A reduction in the total baking time is observed—from approximately 17 minutes in the base case to about 16 minutes. In response to the described conditions, the curve shown in Figure 13 was obtained by modifying the following base-case parameters: (a) the convective heat transfer coefficient, decreased from 25 to 21 W m^{-2} K^{-1}; (b) the radiative flux, reduced from 1900 to 1500 W m^{-2}; and (c) the phase-change kinetics parameter k_{evap} in the, adjusted from 8.1 x 10^{-3} to 7.5 x 10^{-3} s^{-1}. The decrease in radiative flux reaching the *totopo* in the region closest to the embers is explained by the incidence angle of radiation.

The energy balance for an 8 cm *totopo* in diameter, in the lower oven zone, establishes the contribution of each heat transfer mechanism as follows: radiation, 7238 J (33%); contact, 9463 J (44%); and convection, 5011 J (23%).

Conclusions

This work presents a preliminary study of the *totopo* baking process in traditional ovens. It builds upon a review of specialized food engineering literature to develop a model aimed at assessing the influence of heat and mass transfer mechanisms involved in the process. Experimental data were obtained directly from monitoring the operation of traditional ovens using infrared sensors for surface temperature measurement.

The model incorporates an evaporation kinetics formulation that enables, on one hand, the coupling of differential mass and energy balances, and on the other, the independent treatment of mass transport parameters for each phase. Moreover, the vapor-phase moisture content within the sample domain allows linking internal and external transport at the boundaries in terms of gas-phase pressure or concentration. In the phase-change kinetics, the local evaporation temperature within the *totopo* domain is estimated, and correction factors are introduced to inhibit evaporation induced at temperatures below T_{evap}.

In the operation of traditional ovens, it is not feasible to experimentally track the moisture loss of the *totopo* during baking. However, the coupling between mass and energy balances, along with the significant influence of the evaporation energy, allows the experimental monitoring of *totopo* temperature to serve as a suitable indicator for guiding the process modeling.

As an essential objective, the study characterizes the traditional baking process and its distinctive features by analyzing the relative influence of heat transfer mechanisms by radiation, convection, and contact with the inner oven surface. The results show that radiation and contact mechanisms together contribute approximately 75–80% of the total heat supplied to the *totopo*, while convection accounts for the remaining fraction. The study also identifies the instrumentation required in an experimental traditional oven for a more accurate estimation of the individual contributions of these mechanisms. The model results show that no significant temperature gradients are present within the *totopo*, whereas appreciable concentration gradients are observed in both phases.

Regarding internal mass transport in the vapor phase, the model proposes an effective transport coefficient that combines the influence of temperature with a convective contribution associated with pressure gradients. Although these effects are evidently related—since an increase in temperature leads to a rise in the local vapor pressure—their relative influence changes throughout the baking period, as shown by the results presented. It is also worth noting that the term *diffusive* is not used to describe this transport coefficient, since in the gas phase the medium is essentially water vapor. Therefore, the transport mechanism is not purely molecular, dependent on concentration or partial pressure gradients, but rather convective in nature, associated with total pressure gradients.

In summary, this initial study is conceived as a starting point for a line of research aimed at establishing the foundations for future work. Its ultimate goal is to preserve the distinctive features of the traditional process while guiding technological design and adaptation to make it safer and more efficient. Moreover, the study represents a cultural contribution by documenting and analyzing the traditional ovens used for *totopo* production in the Isthmus of Tehuantepec region.

Acknowledgements

This work was carried out under *Instituto* de *Estudios de la Energía de la Universidad del Istmo Project IEE-02/24 PFI*, with the collaboration and support of *totopo* producers from Juchitán, Oaxaca, through Professor Tomás Chiñas Santiago, representative of the *Unión de Artesanos y Campesinos Tona Taati'*. Special thanks are extended to Doña Teresa de la Cruz Sánchez for kindly granting us access to her home and traditional oven, and for her generous hospitality.

References

Carson, J. K., Willix, J., & North, M. F. (2006). Measurements of heat transfer coefficients within convection ovens. *Journal of Food Engineering*, *72*(3), 293-301. https://doi.org/10.1016/j.jfoodeng.2004.12.010

Cengel, Y. A. and Ghajar, A. J., (2015) *Heat and mass transfer; Fundamentals & Applications*, 5th Edition. McGraw-Hill Education.

Cevoli, C., Panarese, V., Catalogne, C., & Fabbri, A. (2020). Estimation of the effective moisture diffusivity in cake baking by the inversion of a finite element model. *Journal of Food Engineering*, *270*, 109769. https://doi.org/10.1016/j.jfoodeng.2019.109769

Chakraborty, S., & Dash, K. K. (2023). A comprehensive review on heat and mass transfer simulation and measurement module during the baking process. *Applied Food Research*, *3*(1), 100270. https://doi.org/10.1016/j.afres.2023.100270

Demirkol, E., Erdogdu, F., & Palazoglu, T. K. (2006). A numerical approach with variable temperature boundary conditions to determine the effective heat transfer coefficient values during baking of cookies. *Journal of Food Process Engineering*, *29*(5), 478-497. https://doi.org/10.1111/j.1745-4530.2006.00074.x.

Dincer, I. (2010). Heat and mass transfer during food drying. In *Mathematical modeling of food processing* (pp. 253-300). CRC Press.

Doulia, D., Tzia, K., & Gekas, V. (2000). A knowledge base for the apparent mass diffusion coefficient (DEFF) of foods. *International Journal of Food Properties*, *3*(1), 1-14. https://doi.org/10.1080/10942910009524613.

Erbay, Z., & Icier, F. (2010). A review of thin layer drying of foods: theory, modeling, and experimental results. *Critical reviews in food science and nutrition*, *50*(5), 441-464. https://doi.org/10.1080/10408390802437063

Feyissa, A. H., Gernaey, K. V., Ashokkumar, S., & Adler-Nissen, J. (2011). Modelling of coupled heat and mass transfer during a contact baking process. *Journal of food engineering*, *106*(3), 228-235. https://doi.org/10.1016/j.jfoodeng.2011.05.014

Gutiérrez-Martínez, S. M.; Hernández-Varela, J. D.; Chanona-Pérez, J. J.; Méndez-Méndez, J. V.; González-Martínez, H.; Perea-Flores, M. J.; Mendoza-Vázquez, S. A.; González-Victoriano, L. (2024). Study of drying, thermal, shrinkage, and color kinetics using digital and thermographic imaging of potato slices under real-time convective drying. *Revista Mexicana de Ingeniería Química*, *23*(3), Alim24322. https://doi.org/10.24275/rmiq/Alim24322

Heldman, D. R., Lund, D. B., & Sabliov, C. (Eds.). (2018). *Handbook of food engineering*. CRC press.

Iribe-Salazar, R., Gutiérrez-Dorado, R., Ríos-Iribe, É., Carrazco-Escalante, M., Vázquez-López, Y., Hernández-Calderón, Ó., & Caro-Corrales, J. (2018). Modeling of effective moisture diffusivity in corn tortilla baking. *Journal of food science*, *83*(8), 2167-2175. https://doi.org/10.1111/1750-3841.14278

Kayacier, A., & Singh, R. K. (2004). Application of effective diffusivity approach for the moisture content prediction of tortilla chips during baking. *LWT-Food Science and Technology*, *37*(2), 275-281. https://doi.org/10.1016/j.lwt.2003.09.003

Krokida, M., & Saravacos, G. D. (2013). Transport properties in food process design. In *Advances in Food Process Engineering Research and Applications* (pp. 119-137). Boston, MA: Springer US. https://doi.org/10.1007/978-1-4614-7906-2_7

Loan, L. T. K., Tat, T. Q., Minh, P. D. T., Thao, V. T. T., Hoang, P. T. M., Nhi, T. T. Y., Giang, B. L., Phat, D. T., Mansamut, C., & Tai, N. V. (2025). Modeling of dehydration, polyphenol thermal degradation, and rehydration of instant germinated VD20 rice: Mathematical and artificial intelligence model. *Revista Mexicana de Ingeniería Química*, *24*(1), Alim24400. https://doi.org/10.24275/rmiq/Alim24400

López-Saynes, G. (2018). Revaloración del *totopo* (Guetabiguii Yaachi) desde el enfoque de la economía social. El caso de mujeres productoras en Juchitán, Oaxaca Tesis de Maestría, IPN CIDIR, unidad Oaxaca.

Mittal, G. S. (2010). Mass Transfer Basics. In Mathematical Modeling of Food Processing (pp. 89-108). CRC Press.

Ousegui, A., Moresoli, C., Dostie, M., & Marcos, B. (2010). Porous multiphase approach for baking process–Explicit formulation of evaporation rate. *Journal of Food Engineering*, *100*(3), 535-544. https://doi.org/10.1016/j.jfoodeng.2010.05.003

Peters, B., Schröder, E., Bruch, C., & Nussbaumer, T. (2002). Measurements and particle resolved modelling of heat-up and drying of a packed bed. *Biomass and bioenergy*, *23*(4), 291-306. https://doi.org/10.1016/S0961-9534(02)00052-1.

Rosentrater, K. A., Flores, R. A., Richard, T. L., & Bern, C. J. (1999). Physical and nutritional properties of corn masa by-product streams. *Applied Engineering in Agriculture*, *15*(5), 515-523.

Saadatkhah, N., Carillo Garcia, A., Ackermann, S., Leclerc, P., Latifi, M., Samih, S., ... & Chaouki, J. (2020). Experimental methods in chemical engineering: Thermogravimetric analysis—TGA. *The Canadian Journal of Chemical Engineering*, *98*(1), 34-43. https://doi.org/10.1002/cjce.23673

Saravacos, G. D., & Maroulis, Z. B. (2001). *Transport properties of foods*. CRC Press.

Serna-Saldivar, S. O., & Chuck-Hernandez, C. (2019). Food uses of lime-cooked corn with emphasis in tortillas and snacks. In *Corn* (pp. 469-500). AACC International Press. https://doi.org/10.1016/B978-0-12-811971-6.00017-6

Thorvaldsson, K., & Janestad, H. (1999). A model for simultaneous heat, water and vapour diffusion. *Journal of food engineering*, *40*(3), 167-172. https://doi.org/10.1016/S0260-8774(99)00052-7.

Urban, J. L., Vicariotto, M., Dunn-Rankin, D., & Fernandez-Pello, A. C. (2019). Temperature measurement of glowing embers with color pyrometry. *Fire Technology*, 55, 1013-1026. https://doi.org/10.1007/s10694-018-0810-3.

Varzakas, T. & Tzia, C. (Eds.) (2014). Food Engineering Handbook Food Engineering Fundamentals. CRC Press.

Welti-Chanes, J., Vergara-Balderas, F. & Bermudez-Aguirre, D. (2005) Transport phenomena in food engineering: basic concepts and advances. *Journal of Food Engineering* 67(1-2), 113–128. https://doi.org/10.1016/j.jfoodeng.2004.05.053.

Xu, S., & Kerr, W. L. (2012). Modeling moisture loss during vacuum belt drying of low-fat tortilla chips. *Drying Technology*, *30*(13), 1422-1431. https://doi.org/10.1080/07373937.2012.685999